Relaxation dynamics of hot protons in a thermal bath of atomic hydrogen

Andrew S. Clarke and Bernie Shizgal
Department of Chemistry, University of British Columbia, Vancouver, British Columbia, Canada V6T 1Z1
(Received 16 November 1992; revised manuscript received 10 August 1993)

We present a rigorous kinetic theory formulation of the relaxation of hot protons (H^+) in a bath of thermal atomic hydrogen (H). We apply the (well-known) quantum-mechanical scattering theory to (H^+,H) collisions and calculate the differential elastic cross section as a function of collision energy and scattering angle. This calculation includes the effects of both direct and charge-exchange scattering. We then solve the time-dependent Boltzmann equation numerically for the H^+ distribution function with an initial δ-function distribution. We also consider two approximate models for the collision dynamics, each based on the assumption that charge exchange dominates the relaxation and that no momentum is transferred in a collision (the linear-trajectory approximation). The first model uses the Rapp-Francis [J. Chem. Phys. 37, 2631 (1962)] energy-dependent cross section in the exact kernel which defines the Boltzmann collision operator. The second model uses a hard-sphere cross section in an approximate collision kernel. We compare the relaxation behavior calculated with the approximate formulations with the exact solution. We also calculate the mobility of H^+ in H and compare the exact and approximate formulations. This study has applications to processes in astrophysics and aeronomy such as the nonthermal escape of H from planetary atmospheres.

PACS number(s): 05.20.Dd, 05.60.+w

I. INTRODUCTION

The transport processes associated with an ensemble of ions dilutely dispersed in a background of the parent atomic gas, or some other neutral species, is an important problem in chemistry and physics [1] with applications to aeronomy, astrophysics, and other areas [2–5]. Here we consider collisions between protons (H^+) and atomic hydrogen (H) in the energy range from 0 to 10 eV. This is a fundamental problem in collision physics and has been investigated by many workers [6–9], [10]. In a (H^+,H) collision, H^+ can be either directly scattered or converted to a H atom via the charge-exchange reaction

$$H^+ + H \rightarrow H_2^+ \rightarrow H + H^+ . \quad (1)$$

From quantum mechanics, it is in principle impossible to distinguish between direct (H^+,H) and charge-exchange collisions if the nuclear spins have random polarizations. However, since the angular distributions of the products differ from direct scattering in comparison with charge-exchange scattering, it is possible in practice to distinguish the two processes [11].

These charge-exchange collisions are important in the activation of atomic hydrogen in the upper atmospheres of Earth [12], Venus [13,14], and Saturn. At high altitudes (> 500 km) in the earth's atmosphere, a hot proton can be converted to a hot H atom in a charge-exchange collision with another H atom. If the energy of the product H atom is greater than the escape energy, then this process can significantly contribute to the escape flux of atomic hydrogen. There has been considerable research done to date on the contribution of such charge-exchange collisions to the escape flux [12–18]. In many of these papers, a simple collision model for (H^+,H) charge-exchange collisions is employed which assumes that the trajectory of the incoming proton is unperturbed in the collision, that is, the proton trajectory is linear. Equivalently, this *linear-trajectory approximation* (LTA) assumes that the differential cross section is dominated by contributions from large-impact-parameter collisions. This is true for heavy-ion–neutral-atom systems [19] but may not be valid for (H^+,H) collisions at low energies where quantum effects are expected to be important because of the small reduced mass of the system [10].

The collision kinematics, according to the linear-trajectory approximation, are particularly simple. If $\mathbf{c}_1$ ($\mathbf{c}_1'$) and $\mathbf{c}_2$ ($\mathbf{c}_2'$) are the velocities of H^+ and H, respectively, before (after) collision, then the velocities of H^+ and H are interchanged so that $\mathbf{c}_1'=\mathbf{c}_2$ and $\mathbf{c}_2'=\mathbf{c}_1$. Hodges and Breig [16] recently presented a detailed analysis of these charge-exchange collisions and suggested that the linear-trajectory approximation may not be valid for the physical conditions in the high-altitude region of the Earth's atmosphere, the exosphere [18], from which most of the escaping hydrogen originates.

The present paper is directed towards a detailed analysis of the relaxation of a nonequilibrium distribution of protons in a bath of neutral hydrogen atoms. The application to the calculation of the charge-exchange-induced escape from a planetary atmosphere is deferred to a different paper. We outline the rigorous quantum-mechanical calculation of the differential cross section including both direct and charge-exchange contributions. We then solve the time-dependent Boltzmann equation numerically. Our method of solution of the Boltzmann equation involves the expansion of the distribution in the eigenfunctions of the collision operator. The time-dependent distribution function is then expressed as a sum of exponential terms with each term characterized by a different eigenvalue of the collision operator.

The present work provides an opportunity to study the

way in which different kernels in the Boltzmann equation affect the relaxation process. There have been several papers concerned with the construction of model kernels and the way in which the detailed structure of the kernel affects relaxation and transport in different systems [20–26]. The present calculations complement these studies. Much of the work to date on the spectrum of the collision operator in the Boltzmann equation has been restricted to either the hard-sphere cross section [27] or "Maxwell molecules," that is, particles interacting with the polarization potential (which varies as $1/r^4$, where r is the ion–neutral-atom separation). The eigenvalues and eigenfunctions for the latter model are well known [28]. We are therefore interested in how the spectrum of the collision operator, and hence the relaxation to equilibrium, depends on the kernel and the differential cross section.

In Sec. II A, we describe the relaxation dynamics in terms of the Boltzmann equation. The Boltzmann collision operator is given as an integral operator with a well-defined kernel. In Sec. II B we outline the quantum-mechanical calculation of the differential cross section, accounting for both direct and charge-exchange scattering contributions. In Sec. III we describe two approximate models for the relaxation dynamics. The first, referred to as LTA1, uses the Rapp-Francis energy-dependent differential cross section in the Boltzmann collision operator. The second, referred to as LTA2, uses a model kernel with a hard-sphere differential cross section. In Sec. IV we describe the method of solution of the Boltzmann equation. Section V contains our results and a discussion. We describe the calculation of the thermal mobility in the Appendix. Throughout the paper we denote differential cross sections by σ and total cross section by Q.

II. EXACT FORMULATION OF RELAXATION DYNAMICS

A. Boltzmann equation

We consider a nonequilibrium system of protons, denoted by a subscript 1, dilutely dispersed in a bath of hydrogen atoms, denoted by a subscript 2. We assume that the number density n_1 of protons is small compared to the number density n_2 of hydrogen atoms, so that only (H^+,H) collisions need to be considered. Because $n_2 \gg n_1$, the hydrogen atom velocity distribution is a Maxwellian at the temperature T, that is $f_2(\mathbf{c}) = f_2^M(\mathbf{c}) = n_2(m_2/2\pi kT)^{3/2} e^{-m_2 c^2/2kT}$. The Boltzmann equation for the time evolution of the proton velocity distribution function is then given by

$$\frac{\partial f_1(\mathbf{c}_1,t)}{\partial t} = J[f_1]$$

$$= 2\pi \int d\mathbf{c}_2 \int d\chi \sin\chi [f_1(\mathbf{c}_1')f_2^M(\mathbf{c}_2') - f_1(\mathbf{c}_1)f_2^M(\mathbf{c}_2)] \times \sigma(g,\chi) g \ , \tag{2}$$

where $\sigma(E,\chi)$ is the differential elastic cross section, $g = |\mathbf{g}| = |\mathbf{c}_1 - \mathbf{c}_2|$ is the magnitude of the relative collision velocity, $E = \rho g^2/2$ is the collision energy, $\rho = m_1 m_2/(m_1+m_2)$, and χ is the scattering angle in the center-of-mass frame. The quantities $\mathbf{c}_1$ and $\mathbf{c}_2$ are the velocities before a collision and $\mathbf{c}_1'$ and $\mathbf{c}_2'$ are the velocities after a collision. The Boltzmann equation can be rewritten in the form [27]

$$\frac{\partial f_1(\mathbf{c}_1)}{\partial t} = \int d\mathbf{c}\, K(\mathbf{c}_1,\mathbf{c}) f_1(\mathbf{c}) - Z(c_1) f_1(\mathbf{c}_1) \ , \tag{3}$$

where the collision frequency $Z(c_1)$ is given by

$$Z(c_1) = \int d\mathbf{c}\, K(\mathbf{c}_1,\mathbf{c}) f_1^M(\mathbf{c})/f_1^M(\mathbf{c}_1) \ , \tag{4}$$

and $f_1^M(\mathbf{c})$ is a Maxwellian distribution. The kernel $K(\mathbf{c}_1,\mathbf{c})$ is given by [29]

$$K(\mathbf{c}_1,\mathbf{c}) = \frac{2\pi f_1^M(\mathbf{c}) f_2^M(\mathbf{c})}{(2M_2)^4 f_1^M(\mathbf{c})} \int_0^\pi d\chi \sin\chi \csc^4\left(\frac{\chi}{2}\right) |\mathbf{c}-\mathbf{c}_1| \times \exp\left[-\frac{m_2}{2kT}\left\{\frac{(1-2M_2)}{M_2}\mathbf{c}\cdot(\mathbf{c}-\mathbf{c}_1) + (4M_2^2)^{-1}|\mathbf{c}-\mathbf{c}_1|^2\left[\csc^2\left(\frac{\chi}{2}\right) - 4M_1M_2\right]\right\}\right] \times \sigma\left[\frac{|\mathbf{c}-\mathbf{c}_1|}{2M_2}\csc\left(\frac{\chi}{2}\right),\chi\right] I_0\left[\frac{m_2}{2kT}\frac{|\mathbf{c}\times\mathbf{c}_1|}{M_2}\cot\left(\frac{\chi}{2}\right)\right] , \tag{5}$$

where I_0 is the modified Bessel function of order zero, $M_1 = m_1/(m_1+m_2)$, and $M_2 = m_2/(m_1+m_2)$. Because the masses of H^+ and H are nearly identical, we set $m = m_1 = m_2$. Then $M_1 = M_2 = \frac{1}{2}$ and the kernel reduces to the simpler expression

$$K(\mathbf{c}_1,\mathbf{c}) = 2\pi f_2^M(\mathbf{c}_1) \int_0^\pi d\chi \sin\chi \csc^4\left(\frac{\chi}{2}\right) |\mathbf{c}-\mathbf{c}_1| \exp\left\{-\frac{m}{2kT}|\mathbf{c}-\mathbf{c}_1|^2\cot^2\left(\frac{\chi}{2}\right)\right\} \times \sigma\left[|\mathbf{c}-\mathbf{c}_1|\csc\left(\frac{\chi}{2}\right),\chi\right] I_0\left[\frac{m}{kT}|\mathbf{c}\times\mathbf{c}_1|\cot\left(\frac{\chi}{2}\right)\right] . \tag{6}$$

In general, $K(\mathbf{c}_1,\mathbf{c})$ depends only on the magnitudes of the velocities $\mathbf{c}_1$ and $\mathbf{c}$, and $\mu=\cos\theta$, where θ is the angle between $\mathbf{c}$ and $\mathbf{c}_1$. We can then rewrite $K(\mathbf{c}_1,\mathbf{c})$ as $K(c_1,c,\mu)$.

The proton distribution function can be written as an expansion in Legendre polynomials,

$$f_1(\mathbf{c},t)=\sum_{l=0}^{\infty} f_1^l(c,t)P_l(\hat{\mu}) , \tag{7}$$

where $\hat{\mu}=\cos\hat{\theta}$ and $\hat{\theta}$ is the polar angle between $\mathbf{c}$ and some fixed axis in velocity space. We assume that the proton velocity distribution function is isotropic so that $f_1(\mathbf{c},t)=f_1^0(c,t)$, and henceforth we drop the superscript 0 on f_1^0. We can then replace the kernel $K(\mathbf{c}_1,\mathbf{c})$ by the isotropic kernel $K_0(c_1,c)$, where

$$K_0(c_1,c)\equiv 2\pi\int_{-1}^{+1} d\mu\, c^2 K(c_1,c,\mu) . \tag{8}$$

The μ integration must be done numerically for all but the simplest cross sections. The Boltzmann equation for the isotropic distribution is then given by

$$\frac{\partial f_1(c_1)}{\partial t}=\int_0^{\infty} dc\, K_0(c_1,c)f_1(c)-Z(c_1)f_1(c_1) . \tag{9}$$

The time evolution of an isotropic, nonequilibrium distribution of protons is given by the solution of the time-dependent Boltzmann equation, Eq. (9), with the differential cross section discussed in the next section. We refer to this kernel $K_0(c_1,c)$ as the *exact* kernel; note that it depends in a complicated way on the detailed structure of the differential cross section.

B. Exact differential cross section

For a detailed description of the quantum-mechanical calculation of the differential scattering cross section for (H^+,H) collisions, we refer the reader to the literature [10, 16, 30–32]. Here we merely summarize the relevant results and outline the calculation of the differential cross section.

At collision energies below approximately 10.2 eV, a complete description of the scattering process requires inclusion of only two electronic states of the H_2^+ ion, namely, the gerade (or $1S_{\sigma_g}$) and ungerade (or $2P_{\sigma_\mu}$) states. The differential cross section is given in terms of the gerade and ungerade scattering amplitudes $f_{g,u}$, which are in turn functions of the quantum-mechanical phase shifts $\delta_l^{g,u}$. Here (a subscript or superscript) g refers to the gerade state and u refers to the ungerade states. The differential cross section $\sigma(E,\chi)$ can then be written uniquely as the sum of two terms, one involving f_g+f_u and one involving f_g-f_u. Terms with f_g+f_u correspond to direct elastic scattering (without charge transfer) and terms with f_g-f_u correspond to scattering with charge exchange [10,16,32]. Thus we can decompose the differential cross section into direct (D) and charge-exchange (CE) parts:

$$\sigma(E,\chi)=\sigma_D(E,\chi)+\sigma_{\mathrm{CE}}(E,\chi) . \tag{10}$$

The *total* cross section is given by

$$\begin{aligned} Q(E)&=2\pi\int_0^{\pi} d\chi\sin(\chi)\sigma(E,\chi)\\ &=2\pi\int_0^{\pi} d\chi\sin\chi\{\sigma_D(E,\chi)+\sigma_{\mathrm{CE}}(E,\chi)\}\\ &=Q_D(E)+Q_{\mathrm{CE}}(E) . \end{aligned} \tag{11}$$

One can show [10,32] that the direct and charge-exchange total cross sections are exactly equal to each other, i.e., $Q_D(E)=Q_{\mathrm{CE}}(E)$. The total momentum-transfer cross section, $Q_m(E)$, defined by

$$Q_m(E)=2\pi\int_0^{\pi} d\chi\sin\chi(1-\cos\chi)\sigma(E,\chi) , \tag{12}$$

is very sensitive to the angular dependence of the differential cross section. For a hard-sphere differential cross section, Q_m is simply equal to the total cross section Q. If the differential cross section is sharply peaked in the forward direction (near $\chi=0$) then Q_m can be much less than Q. On the other hand, if the differential cross section is sharply peaked in the backward direction (near $\chi=\pi$) then Q_m can be as large as $2Q$ (this is shown explicitly in Sec. III).

In our calculations we employed the gerade and ungerade potentials previously calculated by Peek [33] and Wind [34]. We used a cubic-spline routine to interpolate between their data points to ensure a smooth fit. At large internuclear separation ($r>30$), we used the asymptotic formula $V_{u,g}(r)\simeq -9/(4r^4)$. For the gerade potential at small r, we used the Bethe perturbation formula, given by $V_g(r)\simeq 1/r-1.5+8/3r^2$. For the ungerade potential, we used the results of Bates, Ledsham, and Stewart [35] to obtain an approximate formula for $r<0.2$, that is, $V_u(r)\simeq 1/r-0.066\,875r^2$.

At low energies ($E\leq 0.05$ eV) we calculated all the phase shifts by directly integrating the radial Schrödinger equation using a Runge-Kutta-Gill method. At intermediate energies ($0.05\leq E\leq 1.0$ eV) we calculated the low-order phase shifts (up to $l=50$) by direct integration of the radial Schrödinger equation, and we calculated the higher-order ($l>50$) phase shifts semiclassically with the WKB approximation [36]. In the intermediate-energy range, the two different methods agree within approximately 1% for the $l=50$ gerade and ungerade phase shifts. At the highest energies ($E\geq 1.0$ eV) we calculated all of the phase shifts using the semiclassical formula, retaining as many as 300 phase shifts.

We compared our phase shifts and total cross sections with those of Hunter and Kuriyan [30,31]. At high energies and large l, we find excellent agreement with their results, but for small l we find discrepancies of the order of 0.01π in the lowest-order phase shifts, leading to a disagreement of the order of a few percent in the low-energy cross sections. Davis and Thorson [10], and Hodges and Breig [16,37], find similar (small) discrepancies between their calculated phase shifts and those reported by Hunter and Kuriyan. Figure 1 shows our calculated direct and charge-exchange differential scattering cross sections as a function of the center-of-mass scattering angle χ for two different energies. As anticipated, the direct cross section is sharply peaked near $\chi=0$, whereas the charge-exchange cross section is sharply peaked near $\chi=\pi$. As the energy increases, the differential cross sec-

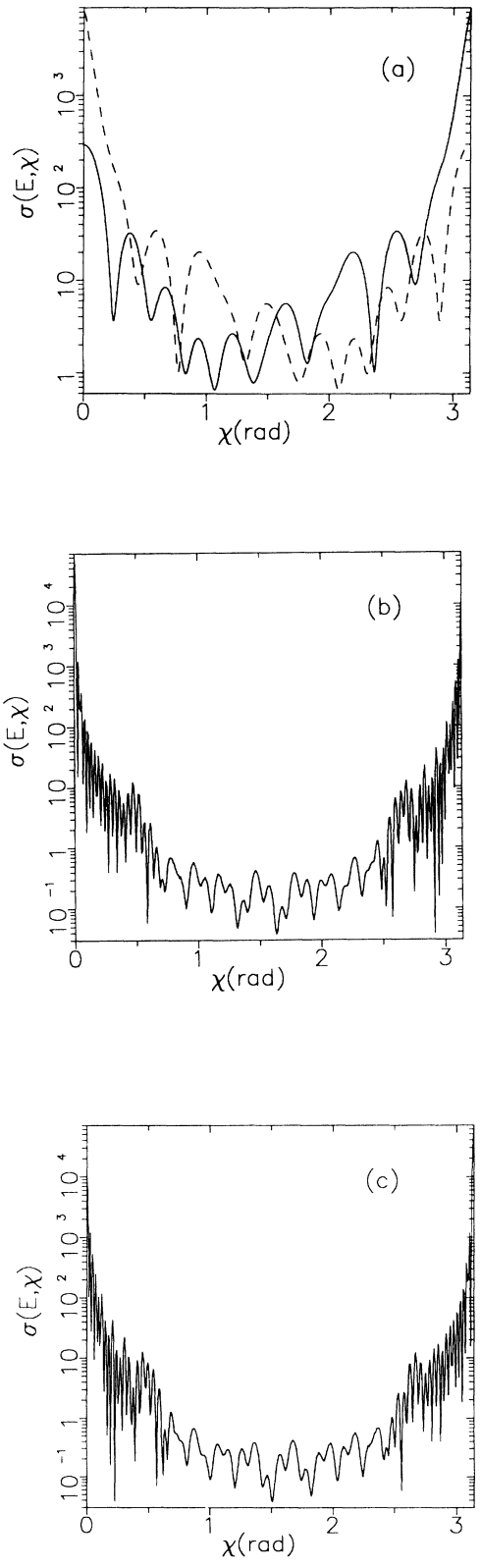

FIG. 1. Direct (D) and charge-exchange (CE) differential cross sections for (H^+,H) scattering, as a function of scattering angle χ, for two different collision energies E. In Fig. 2(a) CE is a solid line and D is a dashed line. (a) D and CE at $E=10^{-2}$ eV. (b) D at $E=5.0$ eV. (c) CE at $E=5.0$ eV.

tions oscillate more rapidly, and the peaks at $\chi=0$, (direct) and $\chi=\pi$ (charge exchange) become sharper.

III. LINEAR TRAJECTORY APPROXIMATION

The exact theory for the relaxation of hot H^+ in a background of H atoms is described in the preceding section. It is also possible to derive several different *approximate* models of the relaxation based on the linear-trajectory approximation discussed in the Introduction. We now describe two such models, which we denote by LTA1 and LTA2. Many of the geophysical models employed to estimate the escape flux of H^+ from planetary atmospheres have used the linear-trajectory approximation. This was questioned by Shizgal [17] and more recently by Hodges and Breig [16]. The present work is directed towards a more detailed study of this approximation.

A. Rapp-Francis model (LTA1)

Based on the linear-trajectory approximation, Rapp and Francis [19] derived an energy-dependent total charge-exchange cross section, which we denote by $Q_{RF}(E)$. At high collision energies the probability of charge exchange as a function of impact parameter, $P(b)$, oscillates rapidly between 0 and 1 for $0<b<b_1$, and decays exponentially with increasing b for $b>b_1$. Rapp and Francis approximate $P(b)$ by its average value of $\frac{1}{2}$ for $b\leq b_1$, and set $P(b)=0$ for all $b>b_1$. The total charge-exchange cross section is then given by

$$Q_{RF}=\tfrac{1}{2}\pi b_1^2 , \tag{13}$$

where, for (H^+,H) collisions, b_1 is the solution to the equation [19]

$$\left[\frac{2\pi}{a_0}\right]^{1/2}\left[\frac{I}{\hbar g}\right]b_1^{3/2}\left[1+\frac{a_0}{b_1}\right]\exp\left[-\frac{b_1}{a_0}\right]=\frac{\pi}{6} . \tag{14}$$

Figure 2 shows the Rapp-Francis total charge-exchange cross section as a function of energy, compared with the exact total charge-exchange cross section. Here the Rapp-Francis cross section is denoted by LTA1, and the charge-exchange cross section is denoted by CE. The Rapp-Francis cross section lies below the exact cross section over the entire energy range, and approaches the exact cross section as the energy increases. Rapp and Francis estimated that their model cross section [for (H^+,H) collisions] is valid over the range $3\times10^{-3}<E<3\times10^{3}$ eV. Figure 3 shows that the relative error, defined by $(Q_{RF}/Q_{CE}-1)$, is approximately 2 for $10^{-1}<E<10$ eV, and increases rapidly with decreasing energy below 10^{-1} eV.

The LTA1 approximate formulation consists of solving the Boltzmann equation, Eq. (9), with the exact kernel, Eqs. (6) and (8), and an approximate differential cross section defined by $\sigma_{LTA1}(E,\chi)=Q_{RF}(E)/4\pi$. Thus the only difference between the exact formulation and the LTA1 formulation is that different differential cross sections are used. The LTA1 formulation replaces the exact differential cross section with an isotropic cross section

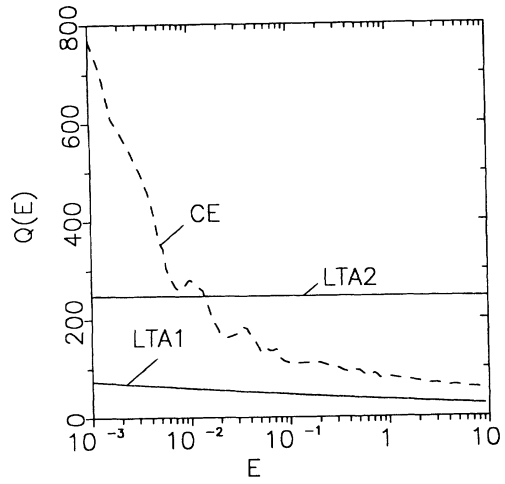

FIG. 2. Total cross section as a function of collision energy E. The total quantum-mechanical charge-exchange (CE) cross section is equal to the total direct (D) cross section (dashed line). The Rapp-Francis (LTA1) total charge-exchange cross section (solid line) and the LTA2 total cross section (horizontal solid line) are also shown.

given by the Rapp-Francis total charge-exchange cross section (divided by 4π).

B. LTA2 Model

The LTA2 formulation consists of a model kernel based on the linear-trajectory approximation, combined with a hard-sphere total cross section (specifically, $\sigma_{\rm HS}=Q_{\rm HS}/4\pi$, where $Q_{\rm HS}$ is independent of both angle and energy). The collision term in the Boltzmann equation, $J[f_1]$ in Eq. (2), becomes

$$J[f_1]=Q_{\rm HS}\int d\mathbf{c}_2[f_1(\mathbf{c}_1')f_2^M(\mathbf{c}_2')-f_1(\mathbf{c}_1)f_2^M(\mathbf{c}_2)]g \ . \tag{15}$$

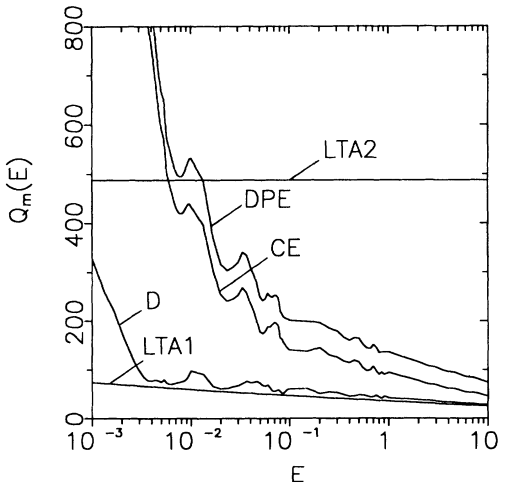

FIG. 3. Total momentum-transfer cross section as a function of collision energy E. The exact total momentum-transfer cross section (DPE) equals the sum of the direct (D) and charge-exchange (CE) contributions. The LTA1 total momentum-transfer cross section is equal to the LTA1 total cross section, and the LTA2 total momentum-transfer cross section is twice the LTA2 total cross section. (See Fig. 2.)

Imposing the linear-trajectory approximation, namely, $\mathbf{c}_1'=\mathbf{c}_2$ and $\mathbf{c}_2'=\mathbf{c}_1$, we obtain

$$J[f_1]=\int d\mathbf{c}\,\tilde{K}(\mathbf{c}_1,\mathbf{c})f_1(\mathbf{c})-\tilde{Z}(c_1)f_1(\mathbf{c}_1) \ , \tag{16}$$

where the approximate kernel $\tilde{K}$ is defined by

$$\tilde{K}(\mathbf{c}_1,\mathbf{c})=Q_{\rm HS}f_2^M(\mathbf{c}_1)|\mathbf{c}-\mathbf{c}_1| \tag{17}$$

and the approximate collision frequency $\tilde{Z}$ is given by

$$\tilde{Z}(c_1)=Q_{\rm HS}\int d\mathbf{c}\,f_2^M(\mathbf{c})|\mathbf{c}-\mathbf{c}_1| \ . \tag{18}$$

The Boltzmann equation thus has the same form as Eq. (9), but now the approximate kernel $\tilde{K}(\mathbf{c}_1,\mathbf{c})$ [38] is much simpler than the exact kernel, Eq. (6). As in Sec. I, we assume the distribution function f_1 is isotropic, and rewrite $\tilde{K}(\mathbf{c}_1,\mathbf{c})$ as $\tilde{K}(c_1,c,\mu)$, where μ is the cosine of the angle between $\mathbf{c}_1$ and $\mathbf{c}$. We then define an isotropic kernel $\tilde{K}_0(c_1,c)$ by

$$\tilde{K}_0(c_1,c)\equiv 2\pi\int_{-1}^{+1}d\mu\,c^2\tilde{K}(c_1,c,\mu) \ , \tag{19}$$

and the Boltzmann equation becomes

$$\frac{\partial f_1(c_1)}{\partial t}=\int_0^\infty dc\,\tilde{K}_0(c_1,c)f_1(c)-\tilde{Z}(c_1)f_1(c_1) \ . \tag{20}$$

Because the differential cross section is a constant, the angular integration in Eq. (19) is easily evaluated, with the result that

$$\tilde{K}_0(c_1,c)=\Gamma(c_1,c)f_2^M(c_1) \ , \tag{21}$$

where

$$\Gamma(c_1,c)=\frac{2\pi Q_{\rm HS}c(|c_1+c|^3-|c_1-c|^3)}{3c_1} \ . \tag{22}$$

The collision frequency $\tilde{Z}(c_1)$ is then calculated numerically [in analogy with Eq. (4)] using

$$\tilde{Z}(c_1)=\int_0^\infty dc\,\tilde{K}_0(c_1,c)f_1^M(c)/f_1^M(c_1) \ . \tag{23}$$

Thus the LTA2 approximate formulation is given by solving the Boltzmann equation, Eq. (20), with the kernel and collision frequency given by Eqs. (21)–(23).

The linear-trajectory approximation is equivalent to allowing only perfect backscattering, that is, $\chi=\pi$. Thus we should be able to derive the LTA2 kernel from the exact kernel, Eq. (6). We now show this explicitly. We therefore define a model differential cross section $\sigma_*(\chi)$ by

$$\sigma_*(\chi)=\frac{Q_{\rm HS}}{2\pi}\frac{\delta(\chi-(\pi-\epsilon))}{\sin(\pi-\epsilon)} \ , \tag{24}$$

where ϵ is a positive number between 0 and π, and $Q_{\rm HS}$ is a hard-sphere total cross section. The differential cross section σ_* incorporates the linear-trajectory approximation in the limit $\epsilon\to 0+$, since that corresponds to backward scattering, i.e., $\mathbf{c}_1'=\mathbf{c}_2$ and $\mathbf{c}_2'=\mathbf{c}_1$. Integrating Eq. (24) over the solid angle we find the total cross section is $Q_{\rm HS}$ for any ϵ in $(0,\pi)$. One can also verify by direct substitution of Eq. (24) into Eq. (12) that the total momentum-transfer cross section is given by

$$Q_m=[1-\cos(\pi-\epsilon)]Q_{\rm HS} \ . \tag{25}$$

If $\epsilon\rightarrow\pi^-$ then $\sigma_*(\chi)$ becomes a δ function at $\chi=0^+$, and $Q_m\rightarrow 0$. On the other hand, if $\epsilon\rightarrow 0+$, $\sigma_*(\chi)$ becomes a δ function at $\chi=\pi^-$, and $Q_m\rightarrow 2Q_{\rm HS}$. Thus Q_m can range from 0 to $2Q$. If we now substitute $\sigma_*(\chi)$ into Eq. (6) then $K(\mathbf{c}_1,\mathbf{c})$ simplifies, yielding

$$K(\mathbf{c}_1,\mathbf{c})=Q_{\rm HS}f_2^M(\mathbf{c}_1)\csc^4\left[\frac{\pi-\epsilon}{2}\right]|\mathbf{c}-\mathbf{c}_1| \times\exp\left\{-\frac{m}{2kT}|\mathbf{c}-\mathbf{c}_1|^2\cot^2\left[\frac{\pi-\epsilon}{2}\right]\right\} \times I_0\left[\frac{m}{kT}|\mathbf{c}\times\mathbf{c}_1|\cot\left[\frac{\pi-\epsilon}{2}\right]\right] . \tag{26}$$

Taking the limit $\epsilon\rightarrow 0+$ and using the fact that $I_0(0)=1$, we explicitly obtain Eq. (17).

Figure 3 shows the total momentum-transfer cross section for all three formulations (exact, LTA1, LTA2), as well as the exact charge-exchange and direct contributions to the total momentum-transfer cross section. Although the total exact charge-exchange and direct cross sections are equal to each other, this equality does not hold in general for the momentum-transfer cross sections. Because charge exchange is much more effective in transferring momentum, the charge-exchange momentum-transfer cross section is much larger than the direct momentum-transfer cross section. In the LTA1 formulation, the differential cross section is independent of angle so that the total momentum-transfer cross section equals the total cross section.

V. SOLUTION OF THE BOLTZMANN EQUATION

If we define a dimensionless speed by $x\equiv v/v_0$, where $v_0=(2kT/m)^{1/2}$, then the Boltzmann equation can be rewritten in dimensionless form as

$$\frac{\partial f_1(x,\tau)}{\partial\tau}=\int_0^\infty dy\, K_0(x,y)f_1(y,\tau)-Z(x)f_1(x,\tau) \ . \tag{27}$$

Here τ is a dimensionless time, defined by $\tau=At$, where $A\equiv 4\pi n_2\sigma_0(2kT/\pi m)^{1/2}$ and $\sigma_0\equiv 1$ Å^2. The dimensionless distribution function $f_1(x,\tau)$ is normalized by $\int_0^\infty dx\, x^2 f_1(x,\tau)=1$ for all $\tau\geq 0$. The dimensionless kernel $K_0(x,y)$ is given explicitly by

$$K_0(x,y)=y^2e^{-x^2}\int_{-1}^{+1}d\mu\,\gamma^{1/2}\int_0^\pi d\chi\sin\chi\csc^4(\chi/2)\exp[-\gamma\cot^2(\chi/2)]\frac{\sigma(E,\chi)}{\sigma_0}I_0(\alpha\gamma^{1/2}\cot(\chi/2)) \ , \tag{28}$$

where $\gamma\equiv(x^2+y^2-2xy\mu)$, $\alpha\equiv 2xy(1-\mu^2)^{1/2}/\gamma^{1/2}$, and $E=kT\gamma\csc^2(\chi/2)$. The dimensionless collision frequency $Z(x)$ is given by

$$Z(x)=\int_0^\infty dy\, K_0(x,y)e^{-y^2}/e^{-x^2} \ . \tag{29}$$

We can rewrite Eq. (27) in the form

$$\frac{\partial f_1(x,\tau)}{\partial\tau}=\int_0^\infty dy\, A(x,y)f_1(y,\tau) \ , \tag{30}$$

where

$$A(x,y)\equiv K_0(x,y)-Z(x)\delta(x-y) \ . \tag{31}$$

The corresponding eigenvalue problem is

$$\int_0^\infty dy\, A(x,y)\psi^{(n)}(y)=-\lambda_n\psi^{(n)}(y) \ . \tag{32}$$

Because $A(x,y)$ is not symmetric in x and y, we consider the *associated* eigenvalue problem defined by

$$\int_0^\infty dy\, B(x,y)\phi^{(n)}(y)=-\lambda_n\phi^{(n)}(y) \ , \tag{33}$$

where

$$B(x,y)\equiv\frac{x}{y}e^{(x^2-y^2)/2}A(x,y) \tag{34}$$

and

$$\phi^{(n)}(x)\equiv xe^{x^2/2}\psi^{(n)}(x) \ . \tag{35}$$

Since $B(x,y)$ is symmetric in x and y, it is easy to show that the $\{\phi^{(n)}(x)\}$ are orthogonal on the interval $[0,\infty)$ with unit weight function. The orthonormal set $\{\phi^{(n)}(x)\}$ then satisfies

$$\int_0^\infty dx\,\phi^{(n)}(x)\phi^{(m)}(x)=\delta_{mn} \ . \tag{36}$$

If we then substitute Eq. (35) into Eq. (36), we obtain the orthonormality condition for the Boltzmann equation eigenfunctions, namely,

$$\int_0^\infty dx\, R(x)\psi^{(n)}(x)\psi^{(m)}(x)=\delta_{mn} \tag{37}$$

with $R(x)\equiv x^2e^{x^2}$.

In general [27], all eigenvalues below $Z(0)$ are discrete, and all eigenvalues above $Z(0)$ are continuous. The continuum eigenfunctions satisfy

$$\int_0^\infty dx\, R(x)\psi(\lambda,x)\psi(\lambda',x)=\delta(\lambda-\lambda') \tag{38}$$

and

$$\int_0^\infty dx\, R(x)\psi(\lambda,x)\psi^{(n)}(x)=0 \ , \quad n\geq 1 \ , \quad \lambda\geq Z(0) \ . \tag{39}$$

The general solution to Eq. (27), subject to the initial condition $f_1(x,\tau=0)=g(x)$, is then

$$f_1(x,\tau)=\sum_{n=1}^\infty a_n\psi^{(n)}(x)e^{-\lambda_n\tau}+\int_0^\infty d\lambda\, a(\lambda)\psi(\lambda,x)e^{-\lambda\tau} \ , \tag{40}$$

with generalized Fourier coefficients a_n and $a(\lambda)$ given by

$$a_n = \int_0^\infty dx\, R(x) g(x) \psi^{(n)}(x) \tag{41}$$

and

$$a(\lambda) = \int_0^\infty dx\, R(x) g(x) \psi(\lambda, x) \ . \tag{42}$$

We solve the Boltzmann equation using the quadrature discretization method (QDM). This method has been described in detail in other papers [39], so we only give an outline here. The basic idea of QDM is to construct a set of orthogonal polynomials $\{P_n(x)\}$ for which the solution of the Boltzmann equation converges rapidly. A Gaussian qaudrature formula of the form

$$\int_0^\infty dx\, w(x) f(x) \approx \sum_{i=1}^N w_i f(x_i) \tag{43}$$

can also be defined, where the points x_i are the roots of $P_N(x)$ and the weights w_i are calculated as described elsewhere [39]. In kinetic theory, the standard choice of basis functions has been the set of Laguerre polynomials, orthogonal with weight function $w(y)=e^{-y}$, where $y=x^2$ is the reduced energy. Another choice is the set of Hermite polynomials, which are orthogonal with weight function $w(x)=e^{-x^2}$. These are not as useful because they are defined on the interval $(-\infty, \infty)$. Shizgal [40] has shown that another choice, the set of "speed polynomials," often provides more rapid convergence of the solutions of the Boltzmann equation. We therefore use the speed polynomials, defined as the *unique* set of orthogonal polynomials $P_n(x)$ which satisfy the orthonormality relation $\int_0^\infty P_n(x) P_m(x) w(x) dx = \delta_{nm}$, where $w(x)=x^2 e^{-x^2}$.

In order to solve for the eigenvalues and eigenfunctions, and then obtain the time-dependent solution using Eqs. (41)–(43), we must first evaluate the kernel K_0 at the (speed) quadrature points. This involves two integrations over μ and χ. We first transform from χ to u using $u^2=\gamma \cot^2(\chi/2)$. Then $(4/\gamma) u\, du = -d\chi \sin\chi \csc^4(\chi/2)$, and the kernel becomes

$$K_0(x,y) = 4y^2 e^{-x^2} \int_{-1}^{+1} d\mu\, \gamma^{-1/2} \times \int_0^\infty du\, u e^{-u^2} \tilde{\sigma}(E,\chi) I_0(\alpha u) \ , \tag{44}$$

where $\tilde{\sigma}(E,\chi)=\sigma(E,\chi)/\sigma_0$, $E=kT(\gamma+u^2)/2$, and $\chi = 2\tan^{-1}(\gamma^{1/2}/u)$. The μ integration is performed using Gaussian quadrature with 100 Legendre points. The integral over u is evaluated using standard (fourth-order) Simpson's rule with 500 equally spaced points.

We calculate the collision frequency using Gaussian quadrature,

$$Z(x_i) = \sum_{j=1}^N w_j K_0(x_i, x_j) / (x_j^2 e^{-x_i^2}) \ , \tag{45}$$

and define the matrix analog of Eq. (31), by replacing the dirac δ function by its discrete quadrature analog, namely, $w(x_j)/w_j \delta_{ij}$. [The corresponding B matrix is given by Eq. (34).] We then define a new matrix C_{ij} as

$$C_{ij} = \left[\frac{w_i w_j}{w(x_i) w(x_j)} \right]^{1/2} B_{ij} \ , \tag{46}$$

and we solve the matrix equation

$$\sum_{j=1}^N C_{ij} \eta_j^{(n)} = -\lambda_n \eta_i^{(n)} \tag{47}$$

subject to

$$\sum_{j=1}^N \eta_j^{(n)} \eta_j^{(m)} = \delta_{mn} \ . \tag{48}$$

The eigenfunctions of the collision operator are then given by

$$\psi_i^{(n)} = w_i^{-1/2} e^{-x_i^2} \eta_i^{(n)} \ . \tag{49}$$

The time-dependent solution to the Boltzmann equation is given by the discrete analog of Eq. (40),

$$f_1(x,\tau) = \sum_{n=1}^N a_n \psi^{(n)}(x) e^{-\lambda_n \tau} \ , \tag{50}$$

with the $\{a_n\}$ evaluated using quadrature in Eq. (41). We solve the Boltzmann equation subject to the initial condition that $g(x)=\delta(x-x')$ and choose x' at one of the quadrature points, say, x_j. Then the discrete form for $g(x)$ is $g(x_n)=w(x_j)/w_j \delta_{nj}$ and the Fourier coefficients are given exactly by $a_n = x_j^2 e^{x_j^2} \psi_j^{(n)}$.

VI. RESULTS AND DISCUSSION

The main objective of the present paper is to study the relaxation dynamics of hot protons in a background of neutral hydrogen atoms, and to investigate the validity of the linear-trajectory approximation. The time-dependent distribution, given by Eq. (50), is represented by a sum of exponential terms, with each term characterized by an eigenvalue λ_n of the linear collision operator. Since the time scale for approach to equilibrium is approximately $1/\lambda_n$, the eigenvalues and equilibration time are related. We first solve for the spectrum of the Boltzmann collision operator with the exact quantum-mechanical cross section. We then repeat this calculation for the direct and charge-exchange cross sections separately, and compare the spectra of both approximate collision operators, LTA1 and LTA2, with the exact spectrum. We calculate the time evolution of the H^+ distribution function for each case assuming an initial δ-function distribution. We also compare the thermal mobility for the exact and approximate formulations.

Table I shows the first five nonzero eigenvalues corresponding to the direct (D), charge-exchange (CE), and direct-plus-charge-exchange (DPE) differential scattering cross sections in the kernel, Eq. (6), in comparison with the results for LTA1 and LTA2. With the exception of LTA2, all of the lower-order eigenvalues shown in this table have converged to approximately three significant figures. Note that the first nonzero eigenvalue λ_2 is much smaller for direct scattering than for charge-exchange scattering; in fact, $\lambda_2^D/\lambda_2^{CE} \simeq 0.285$. Since the near-

TABLE I. Eigenvalues of the Boltzmann collision operator λ_n. Values shown are for $N=100$. The eigenvalues and collision frequency $Z(0)$ are in units of $n_2\sigma_0(32\pi kT/m_1)^{1/2}$, where $\sigma_0=1$ Å^2.

N	λ_2	λ_3	λ_4	λ_5	λ_6	λ_{10}	λ_{15}	$Z(0)$
D	8.65	10.42	11.78	12.70	13.51	15.66	17.40	34.35
CE	30.34	32.21	32.91	33.29	33.51	33.86	34.05	34.08
DPE	38.98	42.64	44.86	46.43	47.53	50.81	53.27	68.42
LTA1	6.78	8.52	8.86	8.90	8.91	9.07	10.26	8.91
LTA2	38.98	38.98	38.99	39.01	39.05	39.58	42.03	38.98

equilibrium relaxation time of the H^+ distribution function is inversely proportional to λ_2, charge exchange is indeed much more effective in slowing down hot protons than direct scattering. Note that the linear-trajectory approximation implicitly assumes that there is no direct scattering so that the ratio $\lambda_2^D/\lambda_2^{CE}$ is effectively zero in the LTA1 and LTA2 approximation.

The LTA1 eigenvalues are much smaller than the corresponding exact (DPE) eigenvalues—the LTA1 formulation underestimates the rate of relaxation. This result may seem surprising since the Rapp-Francis model cross section was derived under the assumption that no momentum is transferred during the charge-exchange process. This would naturally lead to a higher rate than an exact calculation would give, since hot protons would thermalize in a single collision. However, in order to calculate a relaxation rate based on a total cross section, we have used the hard-sphere differential cross section given by $\sigma_{LTA1}(E,\chi)=Q_{RF}(E)/4\pi$. Thus the (unknown) angular dependence of the exact differential cross section is crudely approximated by an isotropic differential cross section. Since the actual differential charge exchange cross section is sharply peaked near $\chi=\pi$, this gives a very poor approximation to the relaxation rate.

The collision frequency at zero speed, $Z(0)$, determines the boundary between the discrete and continuous portions of the spectrum of the collision operator $J[f_1]$. All eigenvalues below $Z(0)$ belong to the discrete spectrum, and "eigenvalues" above $Z(0)$ belong to the continuum. $Z(0)$ is shown in the last column of Table I. Since the differential cross section $Q_{HS}/4\pi$ is an adjustable parameter in the LTA2 formulation, we have chosen $Q_{HS}/4\pi$ so that the first nonzero eigenvalue of the LTA2 collision operator equals the first nonzero eigenvalue of the exact collision operator, that is, $\lambda_2^{LTA2}=\lambda_2^{DFE}$. The total cross section then has the numerical value $Q_{HS}=244$ Å^2. (Note that if we multiply the differential cross section by a constant then the collision frequency and eigenvalues scale correspondingly. If we normalize the eigenvalues by $Z(0)$ then the spectrum of normalized eigenvalues is unchanged by this rescaling.) In the exact and LTA1 formulations, $Z(0)$ clearly exceeds the first few nonzero eigenvalues so that these eigenvalues belong to the discrete portion of the spectrum (the discretum). However, in the LTA2 formulation, we find that $Z(0)$ (calculated with up to 100 quadrature points) equals λ_2 to seven-digit accuracy. If the converged λ_2 equals the converged $Z(0)$, then λ_2 forms the boundary between the discretum and continuum, and there are *no* positive eigenvalues in the discretum. On the other hand, if $\lambda_2<Z(0)$ then there is at least one positive eigenvalue in the discretum. We have not been able to definitively settle this question, but speculate that $Z(0)$ does indeed equal λ_2. If there are no discrete eigenvalues, then the final approach to equilibrium may not be exponential [41].

Whether or not a particular eigenvalue belongs to the discretum or the continuum can often be determined from the convergence of that eigenvalue versus N, the number of quadrature points. Table II shows the convergence of the eigenvalues obtained with the quantum-mechanical (exact) differential cross section. As N increases, the lower eigenvalues listed, which are less than $Z(0)$ and lie in the discretum, appear to be converged by $N=60$. Table III shows the convergence of the eigenvalues of the Boltzmann collision operator with the LTA2 approximation. As N increases, all of the computed nonzero eigenvalues appear to approach (from above) the collision number, $\lambda_2=\tilde{Z}(0)\simeq 38.98$. This suggests that all the LTA2 eigenvalues belong to the continuum since they are all greater than or equal to $Z(0)$.

Figure 4 shows the computed eigenfunctions $x^2\psi^{(n)}$ (for $n=2,4,6$) as a function of reduced speed for the exact (DPE) and LTA1 formulations. The DPE and LTA1 eigenfunctions are smooth functions of x and in each case the nth eigenfunction has n nodes (including the origin). All of the eigenfunctions rapidly approach zero as x increases. The computed LTA2 eigenfunctions (not shown) are sharply peaked about $x=0$, then quickly decay to zero. Although we have confidence in the basic features of the LTA2 eigenfunctions, their accuracy is limited by the small number of points near $x=0$. Shizgal [42] has investigated the continuum eigenfunctions for the hard-sphere collision operator using a quadrature procedure which places a high concentration of points near the origin. He finds that the continuum eigenfunctions oscillate rapidly about zero but do not approach zero as x in-

TABLE II. Convergence of eigenvalues λ_n: Quantum-mechanical cross section (DPE). The eigenvalues are in units of $n_2\sigma_0(32\pi kT/m_1)^{1/2}$, where $\sigma_0=1$ Å^2. The collision frequency $Z(0)$ in these units is 68.43.

N	λ_2	λ_3	λ_4	λ_5	λ_6	λ_{10}	λ_{15}
20	38.91	42.41	44.30	45.67	46.18	51.20	72.70
40	38.94	42.56	44.65	46.14	47.04	49.18	53.93
60	38.97	42.59	44.77	46.31	47.33	50.20	52.26
80	38.98	42.62	44.82	46.38	47.45	50.58	52.67
100	38.98	42.64	44.86	46.43	47.53	50.81	53.27

TABLE III. Convergence of approximate (LTA2) eigenvalues λ_n. The eigenvalues are in units of $n_2\sigma_0(32\pi kT/m_1)^{1/2}$, where $\sigma_0=1$ Å^2. The collision frequency $Z(0)=38.98$ in these units.

N	λ_2	λ_3	λ_4	λ_5	λ_6	λ_{10}	λ_{15}
20	39.04	39.40	40.49	42.83	46.84	79.76	141.33
40	38.99	39.03	39.17	39.49	40.08	47.34	71.14
60	38.98	39.00	39.04	39.13	39.31	41.68	51.44
80	38.98	38.99	39.00	39.04	39.12	40.14	44.73
100	38.98	38.98	38.99	39.01	39.05	39.58	42.03

creases in contrast with our results for the LTA2 model.

Figure 5 shows the time evolution of the H^+ distribution function for an initial δ-function distribution with an energy of 0.646 eV (this corresponds to $x=5.01$ in the figure). This solution, expressed by Eq. (50), was obtained using the Boltzmann equation and the exact (DPE) differential cross section. Notice that the distribution function is bimodal with peaks at the initial and thermal energies. Hot protons are quickly thermalized by charge exchange. Figure 6 shows the time evolution of the H^+ distribution function obtained using the LTA1 formulation. The initial condition is the same as in Fig. 5. The exact differential cross section is sharply peaked near

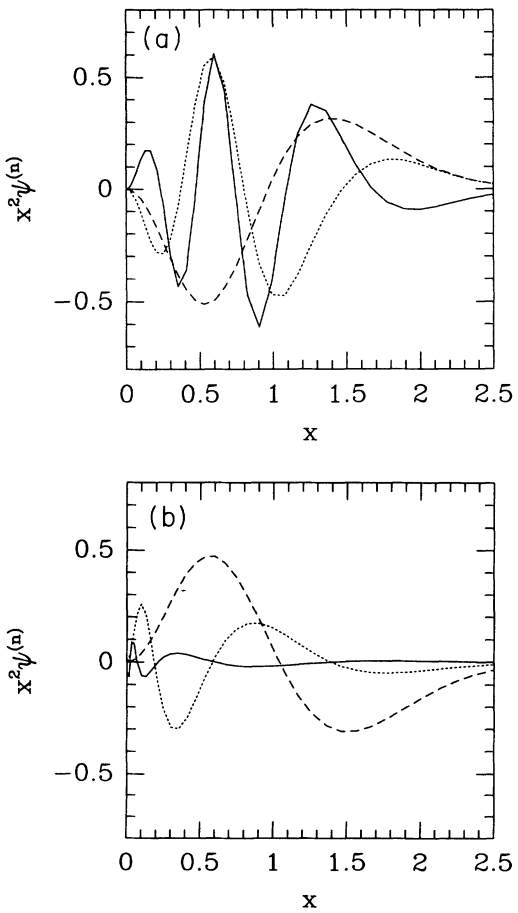

FIG. 4. Eigenfunctions $x^2\psi^{(n)}$ plotted as a function of reduced speed: solid line ($n=2$), dotted line ($n=4$), dashed line ($n=6$). (a) Exact (DPE). (b) LTA1.

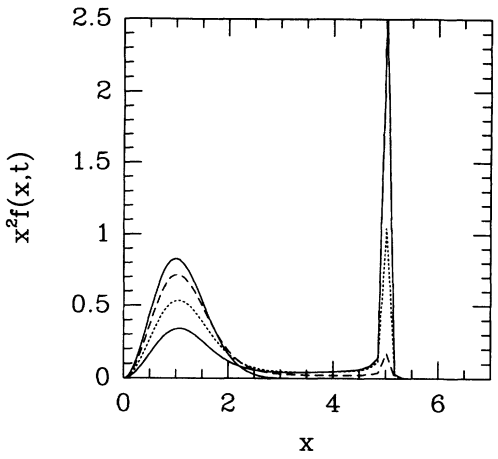

FIG. 5. Time evolution of the H^+ distribution function for an initial δ function at 0.646 eV. Results were obtained from the Boltzmann equation with the exact (DPE) differential cross section. The time t is in units of $n_2\sigma_0(32\pi kT/m)^{1/2}$, where $\sigma_0=1$ Å^2. The curves correspond to $t=0.01$ (solid line), 0.02 (dotted line), 0.04 (dashed line), and 1.0 (solid line).

$\chi=\pi$, making it effective at thermalizing high-energy protons. The LTA1 differential cross section, on the other hand, is independent of angle, and thus exhibits very different relaxation behavior from that shown in Fig. 5. Instead of the direct transfer of energy from initial to thermal energies, in the LTA1 formulation energy transfers occurs gradually. Figure 7 shows the time evolution of the same initial distribution, now calculated using the LTA2 formulation with $Q_{HS}=244$ Å^2. The relaxation behavior is similar to that of Fig. 5.

Figure 8 shows the time evolution of $E(t)/E_{\text{thermal}}$, the ratio of the average proton energy at time t to the average proton energy at the bath temperature. The five curves shown correspond to direct (D) scattering, charge-exchange (CE) scattering, direct-plus-charge-exchange (DPE) scattering, and the LTA1 and LTA2 formulations.

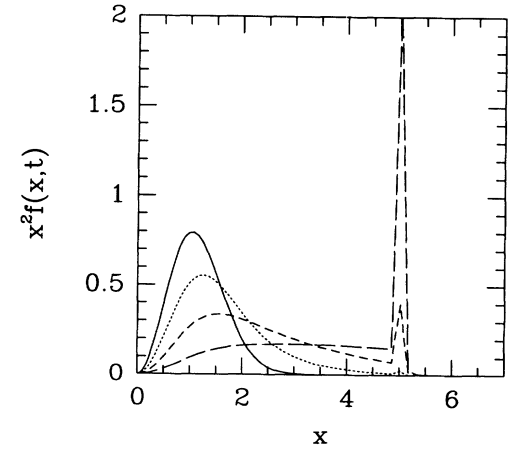

FIG. 6. Time evolution of an initial δ function at 0.646 eV for the approximate LTA1 formulation. The four curves correspond to $t=0.04$ (long-dashed line), 0.10 (short-dashed line), 0.20 (dotted line), and 0.50 (solid line). The units of time are defined in Fig. 5.

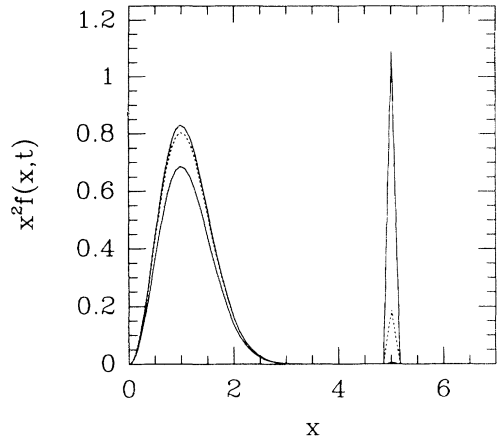

FIG. 7. Time evolution of an initial δ function at 0.646 eV for the approximate Boltzmann equation formulation LTA2. The times are the same as in Fig. 5. The $t=0.04$ (dashed) and $t=1.0$ (solid) curves are nearly indistinguishable on this scale.

In each case the initial proton distribution is a δ function at 0.646 eV. As expected, *D* and LTA1 overestimate the relaxation time since they either ignore or crudely approximate the charge-exchange scattering. On the other hand, CE and LTA2 give much closer approximations to the exact (DPE) relaxation behavior. In order to quantify these differences we define two relaxation times $\tau_{1/e}$ and $\tau_{1.1}$, such that $\tau_{1/e}$ is the time it takes for the energy ratio to decay to $1/e$ of its initial value, the $\tau_{1.1}$ is the time it takes for the energy ratio to decay to 1.1. Table IV shows these relaxation times as a function of initial energy (the initial distribution in each case is a δ function). The rate of approach to equilibrium decreases in the order LTA2, DPE, CE, *D*, LTA1. Note that the shorter time scale $\tau_{1/e}$ is strongly dependent on the initial energy, whereas $\tau_{1.1}$ is nearly independent of initial energy.

In summary, we have described a kinetic theory for the

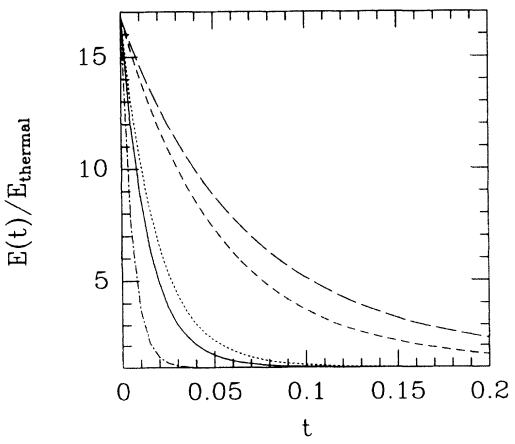

FIG. 8. Time evolution of the average energy per proton $[E(t)]$ divided by the average energy per proton at the bath temperature ($E_{thermal}$) for an initial δ-function distribution at 0.646 eV. Ordered from left to right, the curves are LTA2 (dot-dashed line), DPE (solid line), CE (dotted line), *D* (short-dashed line), and LTA1 (long-dashed line). The units of time *t* are defined in Fig. 5.

TABLE IV. Relaxation times vs initial proton energy. Times are in units of $[n_2\sigma_0(32\pi kT/m_1)^{1/2}]^{-1}$, where $\sigma_0=1$ Å^2.

	$E_0=0.646$ eV		$E_0=1.27$ eV	
	$\tau_{1/e}$	$\tau_{1.1}$	$\tau_{1/e}$	$\tau_{1.1}$
D	0.062	0.336	0.046	0.328
CE	0.022	0.105	0.030	0.101
DPE	0.016	0.080	0.012	0.077
LTA1	0.083	0.498	0.061	0.516
LTA2	0.006	0.029	0.004	0.024

relaxation of a population of hot protons in a bath of thermal atomic hydrogen. We solved the Boltzmann equation numerically for several initial δ-function energy distributions. We also used two approximate calculations of the relaxation dynamics, denoted by LTA1 and LTA2. Both approximate formulations are based on the linear-trajectory approximation, which states that charge-exchange collisions occur without momentum transfer. Of the two approximate models LTA1 and LTA2, the LTA2 model leads to a much better prediction of the relaxation behavior. The LTA1 model uses a poor approximation to the angular dependence of the differential cross section but models the collision energy dependence reasonably well. The LTA2 model uses a poor approximation to the collision energy dependence of the differential cross section, but effectively accounts for the angular dependence. However, the LTA2 formulation, as we show in the Appendix, cannot simultaneously reproduce the correct relaxation behavior and proton mobility. If the LTA2 cross section is chosen so that $\lambda^{LTA2}=\lambda^{DPE}$, then the mobility is approximately a factor of 0.4 too small.

ACKNOWLEDGMENTS

This research was partially supported by grants from the National Science and Engineering Research Council of Canada, and the Petroleum Research Fund administered by the American Chemical Society. We are also grateful to Professor Bob Snider for several useful discussions.

APPENDIX: CALCULATION OF THERMAL MOBILITY

The mobility η of H^+ in a bath of H, is defined as proton drift velocity divided by the electric-field strength ϵ, $\eta=v/\epsilon$. For low electric-field strengths [1,43], the mobility is given by

$$\eta=\frac{3\sqrt{\pi}e}{8(mkT)^{1/2}n_2\bar{Q}_m}\ . \tag{A1}$$

The quantity $\bar{Q}_m$ is an energy-weighted average momentum-transfer cross section, defined by

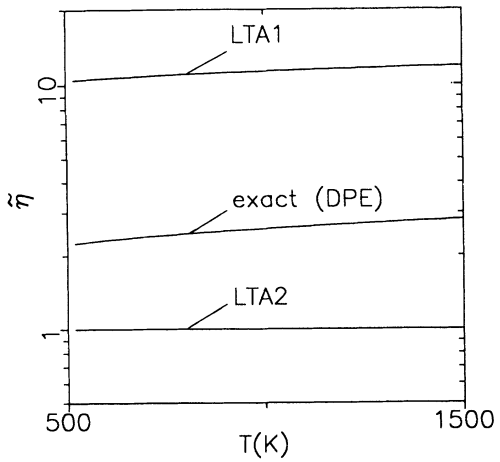

FIG. 9. Dimensionless mobility $\tilde{\eta}$ as a function of hydrogen-bath temperature (T). The dimensionless LTA2 mobility is equal to 1 at all temperatures. The mobility η is given by $B\tilde{\eta}$, where $B \equiv 3e\sqrt{\pi}/16n_2Q_{\rm HS}(mkT)^{1/2}$.

$$\bar{Q}_m \equiv \frac{1}{2(kT)^3}\int_0^\infty dE\, E^2 \exp\{-E/kTQ_m(E)\}\ , \qquad \text{(A2)}$$

and e is the electronic charge.

We define a dimensionless mobility $\tilde{\eta}$ by

$$\tilde{\eta} = \eta/B = \frac{2Q_{\rm HS}}{\bar{Q}_m}\ , \qquad \text{(A3)}$$

where

$$B \equiv \frac{3\sqrt{\pi}e}{16n_2Q_{\rm HS}(mkT)^{1/2}}$$

and $Q_{\rm HS}$ is the total LTA2 cross section, fixed at 244 Å^2. With this normalization, $\tilde{\eta}=1$ in the LTA2 formulation. Figure 9 shows the normalized mobility calculated in the exact, LTA1, and LTA2 formulations versus hydrogen-bath temperature. As one can see from the figure, the LTA1 and LTA2 approximations do not agree with the exact mobility at any temperature. The LTA1 approximation consistently *overestimates* the mobility by a factor of approximately 4, whereas the LTA2 approximation consistently *underestimates* the mobility by a factor of approximately 0.4. The dimensionless LTA2 mobility is independent of temperature; the LTA mobility has a weak temperature dependence similar to that of the exact mobility. This is expected, since the LTA1 differential cross section mimics the energy dependence of the exact differential cross section, whereas the LTA2 differential cross section is independent of energy.

[1] E. W. McDaniel and E. A. Mason, *The Mobility and Diffusion of Ions in Gases* (Wiley-Interscience, New York, 1973); E. A. Mason and E. W. McDaniel, *Transport Properties of Ions in Gases* (Wiley, New York, 1988).

[2] M. H. Rees, *Physics and Chemistry of the Upper Atmosphere* (Cambridge University Press, Cambridge, England, 1989), Chap. 3.

[3] J. R. Stallcop and H. Partridge, Phys. Rev. **32**, 639 (1985).

[4] P. M. Banks and G. Kokarts, *Aeronomy* (Academic, New York, 1973).

[5] R. G. Burnside, C. A. Tepley, and V. B. Wickwar, Ann. Geophys. **5A**, 343 (1987).

[6] E. F. Gurnee and J. L. Magee, J. Chem. Phys. **26**, 1237 (1957).

[7] F. J. Smith, Mol. Phys. **13**, 121 (1967).

[8] F. J. Smith, Proc. Phys. Soc. (London), **92**, 866 (1967).

[9] J. F. Boyle, M. Kennedy, and F. J. Smith, Mol. Phys. **29**, 681 (1975); R. M. Jordon and P. E. Siska, J. Chem. Phys. **69**, 4634 (1978).

[10] J. P. Davis and W. R. Thorson, Can. J. Phys. **56**, 996 (1978).

[11] J. H. Newman, J. D. Cogan, D. L. Ziegler, D. E. Nitz, R. D. Rudd, K. A. Smith, and R. F. Stebbings, Phys. Rev. A **25**, 2976 (1982).

[12] L. J. Maher and B. A. Tinsley, Planet. Space Sci. **26**, 855 (1978); B. A. Tinsley, *ibid.* **26**, 847 (1978); B. Shizgal and M. J. Lindenfeld, J. Geophys. Res. **87**, 853 (1982); J. Chamberlain, *ibid.* **82**, 1 (1977).

[13] B. Shizgal, Adv. Space Res. **12**, 73 (1987).

[14] T. E. Cravens, T. I. Gombosi, and A. Nagy, Nature **283**, 178 (1980); S. Kumar, D. M. Hunten, and J. B. Pollack, Icarus **55**, 369 (1983); J. M. Rodriguez, M. J. Prather, and M. B. McElroy, Planet. Space Sci. **32**, 1235 (1984).

[15] D. M. Hunter and T. M. Donahue, Annu. Rev. Earth Planet. Sci. **4**, 265 (1976).

[16] R. R. Hodges and E. L. Breig, J. Geophys. Res. **96**, 7697 (1991); **98**, 1581 (1993).

[17] B. Shizgal, EOS Trans. Am. Geophys. Union **66**, 1002 (1985).

[18] H. J. Fahr and B. Shizgal, Rev. Geophys. Space Phys. **21**, 75 (1983).

[19] D. Rapp and W. E. Francis, J. Chem. Phys. **37**, 2631 (1962).

[20] E. C. Whipple, J. Chem. Phys. **60**, 1345 (1974); S. Kryszewkii and G. Nienhuis, J. Phys. B **22**, 3435 (1989).

[21] A. K. Prinja, Phys. Fluids **30**, 840 (1987).

[22] A. K. Prinja and M. M. R. Williams, J. Plasma Phys. **44**, 285 (1990).

[23] P. R. Berman, J. E. M. Haverkort, and J. P. Woerdman, Phys. Rev. **34**, 4647 (1986).

[24] R. F. Snider, Phys. Rev. A **33**, 178 (1986).

[25] K. E. Gibble and A. Gallagher, Phys. Rev. A **43**, 1366 (1991).

[26] G. L. Rogers and P. R. Berman, Phys. Rev. A **44**, 417 (1991).

[27] M. R. Hoare, Adv. Chem. Phys., edited by I. Prigogine and S. A. Rice, Vol. XX (1971) 135.

[28] G. W. Ford, Phys. Fluids **11**, 515 (1968); J. Foch and G. W. Ford, in *Studies in Statistical Mechanics*, edited by J. DeBoer and G. E. Uhlenbeck (North-Holland, Amsterdam, 1970), Vol. V.

[29] We derived the kernel using the technique outlined in J. H. Kaper and H. G. Ferziger, *Mathematical Theory of Transport Processes in Gases* (North-Holland, Amsterdam, 1972), pp. 86–93. The same kernel is given by Eq. (2.7) in R. Kapral and J. Ross, J. Chem. Phys. **52**, 3, 1238 (1970).

Note that there is a misprint in Kapral and Ross: the factor (in their notation) $f_2^0(\mathbf{v}_2)$ should be replaced by $f_2^0(\mathbf{v}_1)$.
[30] G. Hunter and M. Kuriyan, Proc. R. Soc. London Ser. A **341**, 491 (1975).
[31] G. Hunter and M. Kuriyan, Proc. R. Soc. London Ser. A **353**, 575 (1977).
[32] L. A. Parcell and R. M. May, Proc. R. Soc. London Ser. A **91**, 54 (1967).
[33] J. A. Peek, J. Chem. Phys. **43**, 9, 3004 (1965).
[34] H. Wind, J. Chem. Phys. **42**, 7, 2371 (1965).
[35] D. R. Bates, K. Ledsham, and A. I. Stewart, Philos. Trans. R. Soc. London Ser. A **246**, 215 (1953).
[36] J. S. Cohen, J. Chem. Phys. **68**, 1841 (1978).
[37] Hodges and Breig report very accurate calculations of the phase shifts and cross sections for (H^+,H) scattering. They give a detailed comparison of their results with those of Hunter and Kuriyan.
[38] G. H. Wannier, *Statistical Physics* (Wiley, New York, 1966), p. 462. Wannier discusses this model in the limit where the bath temperature is zero.
[39] B. Shizgal, J. Comput. Phys. **41**, 309 (1981); B. Shizgal, M. J. Lindenfeld, and R. Reeves, Chem. Phys. **56**, 249 (1981); R. Blackmore and B. Shizgal, J. Chem. Phys. **83**, 2934 (1985).
[40] B. Shizgal, J. Chem. Phys. **70**, 1948 (1979); **74**, 1401 (1981).
[41] B. Shizgal, Trans. Theory Stat. Phys. **21**, 645 (1992); N. Corngold, Phys. Rev. A **15**, 2454 (1977); **24**, 656 (1981).
[42] B. Shizgal, Can. J. Phys. **62**, 97 (1984).
[43] T. Holstein, J. Phys. Chem. **56**, 832 (1952).